# Conformation Transformation Determined by Different Self-Assembled Phases in a DNA Complex with Cationic Polyhedral Oligomeric Silsesquioxane Lipid

**Li Cui,[†] Daoyong Chen,[‡,*] and Lei Zhu[†,*]**

[†]Polymer Program, Institute of Materials Science and Department of Chemical, Materials and Biomolecular Engineering, University of Connecticut, Storrs, Connecticut 06269 and [‡]Department of Macromolecular Science and Key Laboratory of Molecular Engineering of Polymers, Fudan University, Shanghai 200433, China

**ABSTRACT** In this work, a novel cube-shaped cationic lipid based on the imidazolium salt of polyhedral oligomeric silsesquioxane (POSS) was complexed with double-stranded DNA. Because of the negative spontaneous curvature of the cationic POSS imidazolium lipid, an inverted hexagonal phase resulted above the melting point of POSS crystals. Depending on the competition between the crystallization of POSS molecules and the negative spontaneous curvature of cationic POSS imidazolium lipids, different self-assembled phase morphologies were obtained. A lamellar phase was obtained when the POSS crystallization was relatively slow. When the POSS crystallization was fast, an inverted hexagonal phase was obtained with POSS lamellar crystals grown in the interstitials of DNA cylinders. On the basis of a circular dichroism study, double-stranded DNA adopted the B-form helical conformation in the inverted hexagonal phase, whereas the helical conformation was largely destroyed in the lamellar phase.

**KEYWORDS:** DNA-complexes · cationic lipid · polyhedral oligomeric silsesquioxane · conformation · self-assembly

Besides its storage of rich genetic information, negatively charged double-stranded DNA is a unique biomacromolecule because of its characteristic double-stranded helical conformation and long persistent length (~50 nm).[1] These unique features differentiate DNA from flexible synthetic polyelectrolytes, and have enabled its novel hierarchical ionic self-assembly with a broad range of cationic species, including metal cations, cationic lipids, and cationic proteins or even polymers. These DNA complexes find applications in life,[2] biomedical,[3] and polymer[4,5] sciences. For example, DNA−cationic lipid complexes (or lipoplexes) have recently been found useful for nonviral gene transfection and gene therapy.[3] Developing new DNA−cationic lipid systems and understanding their unique self-assembled structures at the nanoscale therefore become indispensable and challenging research.[6]

Equilibrium nanostructures of DNA lipoplexes, including lamellar and inverted hexagonal phases, are a result of the free energy balance among surface charge density, spontaneous curvature of the lipids, and elastic properties of the lipid bilayers. When the lipid spontaneous curvature ($c_0$) is low (zero) and the bending modulus ($k$) is high, a lamellar phase with parallel DNA chains intercalated between positively charged lipid bilayers (a mixture of cationic and neutral helper lipids) is preferred.[7−9] When the $c_0$ is high (negative and $c_0 \approx 1/R_{DNA}$ where $R_{DNA}$ is the radius of DNA around 1.0 nm) and the $k$ is low, an inverted hexagonal phase is favored.[10]

It has been reported that mesophase morphology of lipoplexes is one of the important factors for high transfection efficiency.[10−12] Controlling transformations between lamellar and inverted hexagonal phases has thus received much attention. The first method is to use a hexagonal forming helper (neutral) lipid, together with lamellar forming cationic lipids. When negatively curved dioleoyl phosphatidylethanolamine (DOPE) mixed with a lamellar cationic lipid, an inverted hexagonal phase formed when the DOPE weight fraction was above 0.65.[10] The second method is to incorporate a short alcohol such as hexanol into the cationic lipids to reduce the bilayer bending rigidity.[10,13−15] With an increase of the hexanol content, a clear lamellar to inverted hexagonal transition was observed. The third method is to tailor the molecular size and shape of the hydrophobic tails in

*Address correspondence to lei.zhu@uconn.edu, chendy@fudan.edu.cn.

Received for review July 28, 2007 and accepted March 31, 2008.

**Published online April 12, 2008.**
10.1021/nn800177v CCC: $40.75

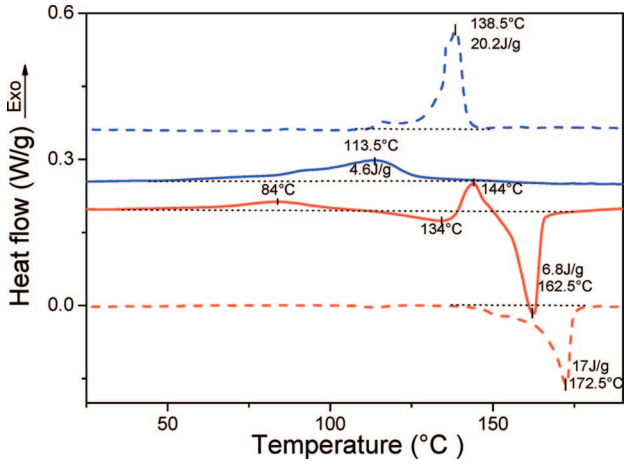


**Figure 1. DSC thermograms of the POSS imidazolium salt and DNA−POSS imidazolium salt complex during the first heating (red curves) and first cooling (blue curves) processes. Dashed curves are for the POSS imidazolium salt and the solid curves are for the DNA−POSS imidazolium salt complex (signals are doubled for better clarity).**

cationic lipids.[16,17] When there was an increase in the tail size and/or change in the tail shape to become more wedge-like, an inverted hexagonal phase was favored.[17] Recently, other methods were also employed to induce the inverted hexagonal morphology. pH-controlled DNA condensation in the presence of dodecyldimethylamine oxide (DDAO) could induce the inverted hexagonal phase at low pH values for the DNA−DDAO complex, but the lamellar phase formed for the DNA−DDAO/DOPE complexes.[18] A thermally reversible lamellar to inverted hexagonal transition was observed in DNA complexes with dodecyltrimethylammonium bromide (DTAB)/DOPE.[19,20] Occasionally, the number and length of lipid tails seemed to affect the mesophase morphology of lipoplexes; some synthetic single-tailed cationic surfactants were favorable for the inverted hexagonal phase.[21,22] Furthermore, a lamellar to inverted hexagonal transition was achieved by DNA induced lipid mixing of some binary liposomes.[23] Finally, anionic lipids together with divalent cations (*e.g.*, $Mg^{2+}$, $Ca^{2+}$, $Mn^{2+}$, *etc.*) were also able to induce DNA condensation, and an inverted hexagonal phase was observed.[24,25]

In a recent communication, it was reported that an inverted hexagonal phase was successfully achieved by using a negatively curved cationic lipid having a cubic tail, namely, polyhedral oligomeric silsesquioxane (POSS) imidazolium salt.[17] However, the fundamental physics for the formation of the inverted hexagonal phase and relationship between DNA−POSS imidazolium salt self-assembly and POSS crystallization were not clearly understood. In this work, we report on pathway dependent phase transitions in the novel self-assembled DNA−inorganic cationic lipid complex, which is determined by the competition between POSS crystallization and negative spontaneous curvature of the cationic lipid. When POSS crystallization overwhelmed the self-assembly process, a lamellar phase was observed. When the negative spontaneous curvature predominated the self-assembly process, an inverted hexagonal phase was obtained. Intriguingly, DNA retained the B-form helical conformation in the inverted hexagonal phase, whereas in the lamellar phase DNA helical conformation was largely destroyed. To the best of our knowledge, no other single DNA lipoplex has been reported so far to exhibit both lamellar and inverted hexagonal phases at ambient temperature, and pathway dependent phase transitions.

## RESULTS AND DISCUSSION

**Thermal Behavior of DNA−POSS Imidazolium Salt Complex.** On the basis of a previous study, 3-hydroxypropyl-heptaisobutyl−POSS (iB-POSS-OH) had a melting point of 136.6 °C.[26] After covalent attachment of an undecanoyl imidazolium salt to iB-POSS-OH, the melting temperature of the POSS imidazolium salt substantially increased, as evidenced by dashed-line differential scanning calorimetry (DSC) curves in Figure 1. Upon first heating, the POSS imidazolium salt had a melting peak at 172.5 °C with a heat of fusion of 17.0 J/g (or 20.4 kJ/mol). Note that this heat of fusion is almost the same as that (19.9 kJ/mol) for pure iB-POSS-OH.[27] Upon first cooling, a crystallization peak was observed at 138.5 °C. Granting that there is a similar heat of fusion but a higher melting point for the POSS imidazolium salt, it is inferred that the entropy change during the crystal melting must be smaller than that for pure iB-POSS-OH crystals, and this can be attributed to the ionic aggregation among the molten imidazolium salts.

DSC first heating and first cooling curves of the DNA−POSS imidazolium salt complex are shown as the solid lines in Figure 1. During heating, besides a small crystallization peak at 84 °C, a minor melting at 134 °C, and an immediate recrystallization at 144 °C, the complexed sample finally melted at 162.5 °C with a heat of fusion of 6.8 J/g. Upon cooling, only a broad crystallization peak was seen at 113.5 °C.

Comparing the thermal behavior of POSS imidazolium salt and its complex with DNA, the latter had a lower melting temperature and a smaller heat of fusion. The smaller heat of fusion could be primarily attributed to the incorporation of noncrystalline DNA in the sample. After normalization to the iB-POSS weight fraction (*ca.* 48 wt % assuming the average negative to positive charge ratio is 3.1; the composition determination can be found in the Supporting Information), the heat of fusion of the POSS crystals was 17.0 kJ/mol, slightly lower than that of the POSS crystals. From the X-ray study below, the DNA−POSS imidazolium salt complex melted (at 162.5 °C) into an inverted hexagonal liquid crystalline phase, instead of an isotropic melt as in the pure POSS imidazolium salt (a polarized optical microscopy study showed the absence of birefrin-

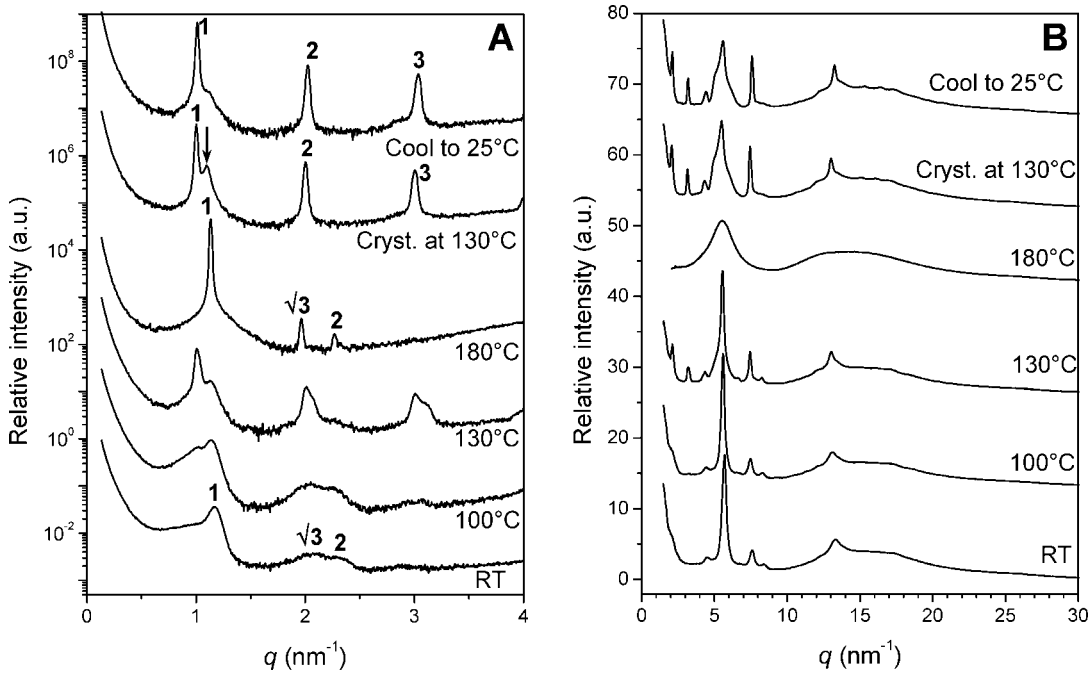


**Figure 2. One-dimensional (A) SAXS and (B) WAXD profiles for the DNA−POSS imidazolium salt complex at different temperatures. At each temperature, the sample was annealed for 5 min before X-ray measurement.**

gence after the salt melted at 172.5 °C). The lower melting temperature (*ca.* 10 °C lower) could be attributed to the incorporation of double-stranded DNA, which decreased the thermodynamic stability of the POSS crystals.

**Supramolecular Self-Assembly in DNA−POSS Imidazolium Salt Complex.** First, negative curvature in the neat POSS imidazolium lipid was proved by small-angle X-ray scattering (SAXS) and wide-angle X-ray diffraction (WAXD) experiments (see the Supporting Information). An inverted hexagonal phase was observed with imidazolium salts forming ionic cylinders in a POSS matrix. The POSS moieties in the matrix crystallized into ABCA four-layer lamellar crystals having an $R\bar{3}m$ symmetry.[27] On the basis of the WAXD result, the unit cell dimensions were determined as $a = 1.62$ nm, $c = 1.72$ nm, and $\gamma = 120°$.

After complexation of the cationic imidazolium salt with negatively charged double-stranded DNA, the self-assembled phase morphology and phase transitions were also studied by SAXS and WAXD. Figure 2 panels A and B show SAXS and WAXD profiles of the DNA−POSS imidazolium salt complex at different temperatures. For the DNA−POSS imidazolium salt complex cast from chloroform solution at room temperature, SAXS showed broad reflections with the *q*-ratio being 1:$\sqrt{3}$:$\sqrt{4}$, indicative of a hexagonally packed cylindrical phase. The *d*-spacing of the (100) reflection was 5.56 nm$^{-1}$, corresponding to an intercylinder distance of 6.42 nm. Meanwhile, the WAXD profile showed distinctive POSS crystal reflections, (10$\bar{1}$1), (11$\bar{2}$0), (10$\bar{1}$2), and (11$\bar{2}$3)/(30$\bar{3}$0). Note that from this WAXD result, the crystal structure and unit cell dimensions kept the same as those for the neat POSS imidazolium lipid. When the sample was heated to 100 °C, a shoulder reflection at a smaller *q* value (*ca.* 1.0 nm$^{-1}$) was seen in the SAXS profile. With further increasing the temperature to 130 °C, this shoulder reflection became sharper and stronger, and higher order reflections with the *q*-ratio being 1:2:3 were clearly observed, suggesting the development of a lamellar crystalline structure. Meanwhile, no substantial change in the POSS crystalline reflections was seen in the WAXD profile, except that the crystalline reflections became slightly sharper and stronger, indicative of a better organized POSS crystalline phase at high temperatures (*e.g.*, 100 °C). This could be correlated to the recrystallization peak in the DSC curve in Figure 1. Finally, POSS crystals melted at 180 °C, and the newly developed crystalline lamellar phase at 130 °C returned to the inverted hexagonal phase, which showed sharp reflection peaks with the *q*-ratio being 1:$\sqrt{3}$:$\sqrt{4}$. The first order reflection was again at 1.13 nm$^{-1}$, which corresponded to an intercylinder distance of 6.42 nm. In the WAXD profile at 180 °C, POSS crystal reflections completely disappeared. Other than the conventional amorphous halo centered around 14.0 nm$^{-1}$, another intense halo was seen at 5.5 nm$^{-1}$ (*d*-spacing = 1.14 nm). Judging from the average *d*-spacing of 1.14 nm, this halo must correspond to the average distance among disordered POSS molecules. With further increasing temperature above 200 °C, DNA would thermally decompose, as evidenced by the disappearance of birefringence under polarized optical microscope and a dark brown appearance of the sample. We speculate that the isotropization temperature of the inverted

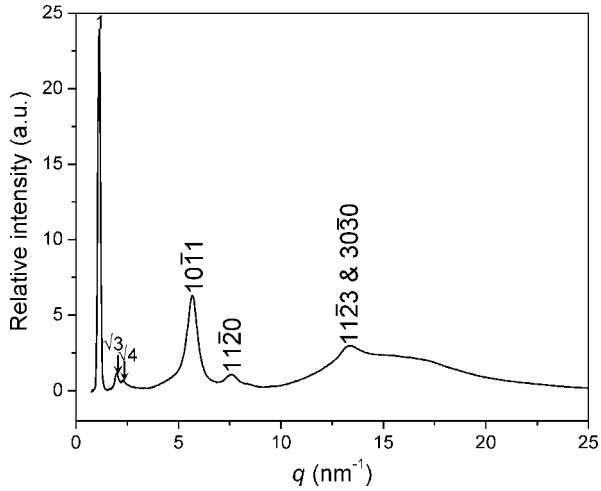


**Figure 3. One-dimensional X-ray diffraction profile of the DNA−POSS imidazolium salt complex quenched from the melt at 180 °C to ice/water at 0 °C.**

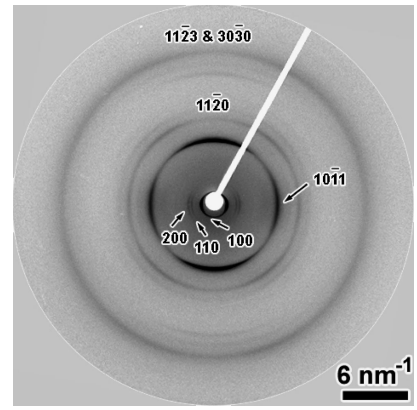


**Figure 4. A two-dimensional X-ray diffraction pattern for shear-oriented DNA−POSS imidazolium salt complex having an inverted hexagonal phase. The shear direction is vertical. The inverted hexagonal phase and trigonal iB-POSS crystal reflections are labeled in the pattern.**

hexagonal phase must exceed its decomposition temperature.

Depending upon different crystallization pathways, distinct crystalline and self-assembled phase morphologies could be achieved. When the DNA−POSS imidazolium salt was cooled from the melt to 130 °C and allowed to crystallize isothermally (see Figure 2 panels A and B), well-defined lamellar reflections were observed with the $q$-ratio being 1:2:3. The first order reflection at 0.98 $nm^{-1}$ had a lamellar spacing of 6.41 nm. It was seen that there was still some residue inverted hexagonal phase, as indicated by the peak with an arrow at $q$ = 1.13 $nm^{-1}$. After being cooled to 25 °C, the residue hexagonal reflection at 1.13 $nm^{-1}$ almost disappeared. In the WAXD profiles in Figure 2B, sharp POSS crystal reflections were seen. Note that the broadening of the POSS (10$\bar{1}$1) reflection is attributed to an overlap with higher order (the fifth and sixth) lamellar reflections. However, if the DNA−POSS imidazolium salt complex was quickly quenched from the melt into ice/water at 0 °C, the inverted hexagonal phase was retained, as evidenced by the X-ray diffraction profile in Figure 3. In the low angle region, the inverted hexagonal phase showed reflections with the $q$-ratio being 1:$\sqrt{3}$:$\sqrt{4}$. In the high angle region, POSS crystal reflections were clearly seen, but with a broader line width than those from the lamellar phase (Figure 2B), suggesting a smaller crystallite size of the POSS crystals due to fast quenching.

On the basis of the above studies, the DNA−POSS imidazolium salt complex could exhibit either an inverted hexagonal (cast from solution or quenched from the melt) or a lamellar (slowly crystallized from the melt) phase, depending upon different crystallization conditions for POSS moieties in the sample. To understand the underlying mechanism for the formation of these self-assembled nanostructures, detailed crystalline and microphase structures of the inverted hexagonal and lamellar phases were studied for shear-oriented samples using 2D X-ray diffraction experiments. Figure 4 shows the two-dimensional (2D) X-ray diffraction pattern of the shear-oriented inverted hexagonal phase. The shear direction was vertical, and inverted hexagonal phase reflections, (100), (110), and (200), centered on the equator, suggesting that double-stranded DNA chains conformed to the shear direction. There were two pairs of (10$\bar{1}$1) reflection arcs centered on both equator and meridian with those on the meridian being stronger. Four (11$\bar{2}$0) reflection arcs were observed in the quadrants, whereas the mixed (11$\bar{2}$3)/(30$\bar{3}$0) reflections did not have discernible orientations.

This 2D X-ray diffraction pattern can be explained using mixed [21$\bar{2}$]- and [635]-uniaxial patterns, as depicted in Figure 5A. Figure 5B shows a real-space arrangement for both POSS crystals and hexagonally packed DNA chains. First, double-stranded DNA aligned vertically in an inverted hexagonal lattice, and thus the (100), (110), and (200) reflections should be on the meridian (Figure 5A). Second, for the [21$\bar{2}$]-uniaxial pattern, the (10$\bar{1}$1) planes aligned nearly perpendicular to the shear direction (Figure 5B), and the (10$\bar{1}$1) reflections should thus appear on the meridian (Figure 5A). Since the angle between the (10$\bar{1}$1) and lamellar basal planes was 51°, POSS lamellar crystals (top right of Figure 5B) oriented at an angle of 39° from the vertical DNA axes. Meanwhile, no (0003)-twin crystal reflections could be observed in the lamellar POSS crystals, because these crystals only had ABCA four layers. Third, for the [635]-uniaxial pattern, the (10$\bar{1}$1) planes oriented parallel to the vertical DNA axes, and thus a pair of (10$\bar{1}$1) reflection arcs should be on the equator. These POSS lamellar crystals oriented at an angle of 51° from the DNA cylinder axes (top left of Figure 5B). Combining the [21$\bar{2}$]- and [635]-uniaxial patterns, the predicted pattern is shown in Figure 5A. Compared with this predicted pattern, the experimental X-ray diffraction pattern in Figure 4 fitted reasonably well. Note that the (11$\bar{2}$0) reflec-

tions around the equator in Figure 4 could possibly result from a small amount of unoriented POSS crystals. Meanwhile, if the crystal orientation was less than perfect, it is likely that no preferred orientation should be seen for the mixed $(11\bar{2}3)/(30\bar{3}0)$ reflections. Fourth, the intensity of the $(11\bar{2}0)$ reflections on the meridian was higher than those on the equator, suggesting that the population of the $[21\bar{2}]$-uniaxial crystals was higher than that of the [635]-uniaxial crystals. Judging from the intensity ratio of the meridian to equator $(10\bar{1}1)$ reflections, the population of the $[21\bar{2}]$-uniaxial crystals was 2.27 times that of the [635]-uniaxial crystals. Since the $[21\bar{2}]$-uniaxial lamella is more or less parallel to the shear direction than the [653]-uniaxial lamella (see Figure 5B), its population should be predominant in the shear-oriented sample. Finally, judging from the relatively poor orientation factor of the $(10\bar{1}1)$ reflections on the meridian, it is likely that a broad distribution of the POSS lamellar orientation existed in the sample.

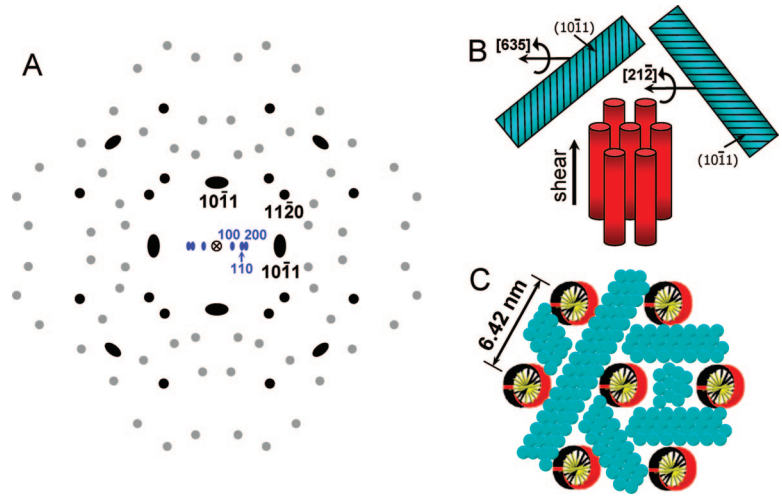


**Figure 5. (A) Predicted mixed [635]- and $[21\bar{2}]$-uniaxial diffraction pattern for iB-POSS lamellar (ABCA four-layer) crystals. The reflections from the hexagonally packed DNA cylinders are labeled with blue (*hkl*) indices, whereas the iB-POSS crystal reflections are labeled with black (*hkil*) indices. Black reflections indicate those observed experimentally, whereas gray reflections are not seen experimentally. A real-space schematic representation of the DNA inverted hexagonal phase (bottom) and iB-POSS crystal orientations (top) is demonstrated in part B. (C) Schematic representation of parallel and hexagonally aligned DNA cylinders and ABCA four-layer POSS lamellar crystals in the interstitials. The view is along the DNA double helix axes.**

The real-space model viewed along the DNA double helices is shown in Figure 5C. Judging from the full-width at half-maximum of the $(10\bar{1}1)$ reflection in Figure 4, its average crystallite size was estimated, using the Scherrer equation,[28] to be 18.2 nm. This distance was much larger than that of the inter-DNA cylinder distance of 6.42 nm, suggesting that the average lateral crystallite size should be greater than 6.42 nm. Therefore, a plausible molecular model is that the POSS lamellar crystals preferentially grow along the {100} interstitials among DNA cylinders (see Figure 5C). However, direct evidence for such an orientation will need single crystal X-ray diffraction of the inverted hexagonal phase and will be subject to future studies.

Figure 6 shows the 2D X-ray diffraction of the oriented DNA−POSS imidazolium salt complex having a lamellar morphology. Here, the sample was obtained by annealing the shear-oriented inverted hexagonal sample at 130 °C for 2 h, because the inverted hexagonal phase could transform into the lamellar phase *via* melt-recrystallization (see DSC and X-ray results in Figures 1 and 2A, respectively). The shear direction was horizontal. Again, the oriented inverted hexagonal phase effectively transformed into the oriented lamellar phase in Figure 6. At low angles, equally spaced lamellar reflections, (001), (002), and (003), were seen to center on the meridian, indicating a horizontal alignment of the lamellae. Sharp POSS $(10\bar{1}1)$ and $(11\bar{2}0)$ reflections were primarily centered on the equator, whereas the rest of the POSS reflections did not show preferred orientation. This 2D X-ray diffraction pattern is similar to those reported previously for a POSS-triphenylene dyad molecule[27] and poly(ethylene)-*b*-poly(ethylene oxide)-*b*-POSS triblock oligomers.[26] To avoid redundancy, here we give a brief explanation of this diffraction pattern on the basis of previous studies. Parallel-aligned DNA and POSS lamellar crystals, which had ABCA four layers, formed alternating layers. When POSS lamellar crystals oriented more or less parallel to the shear direction (strictly speaking, the lamellar crystals oriented at an angle between 0° and 39° with respect to the shear direction[27]), the POSS $(10\bar{1}1)$ reflections should primarily center on the equator, and the overall lamellar reflections [*e.g.*, (001)] should center on the meridian. Such a crystal orientation in the lamellar phase was actually similar to the case of the $[21\bar{2}]$-uniaxial crystals in the shear-aligned hexagonal phase, where they also roughly oriented parallel to the shear direction (see the above discussion). Note that a weak pair of POSS $(10\bar{1}1)$ reflections were seen on the meridian, and they were attrib-

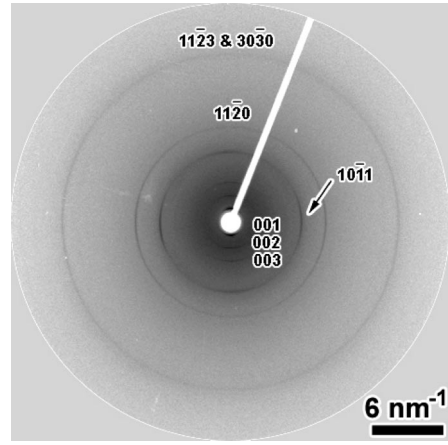


**Figure 6. Two-dimensional X-ray diffraction pattern of oriented DNA−POSS imidazolium salt complex having a lamellar phase. Note that this sample was obtained by annealing the shear-oriented hexagonal sample at 130 °C for 2 h.**

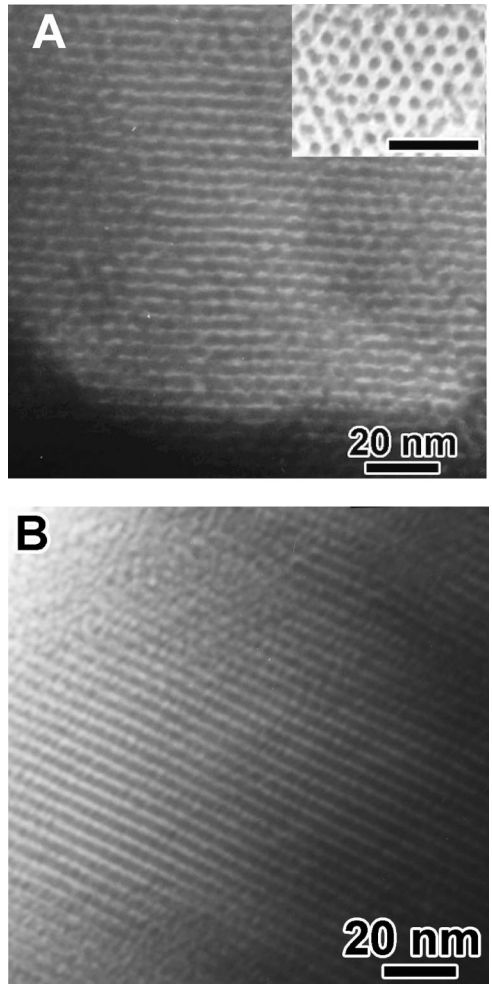


**Figure 7. Bright-field TEM micrographs of the DNA−POSS imidazolium salt complex having (A) the inverted hexagonal and (B) the lamellar phases. The inset of panel A shows a head-on view of hexagonally packed DNA cylinders (scale bar = 20 nm).**

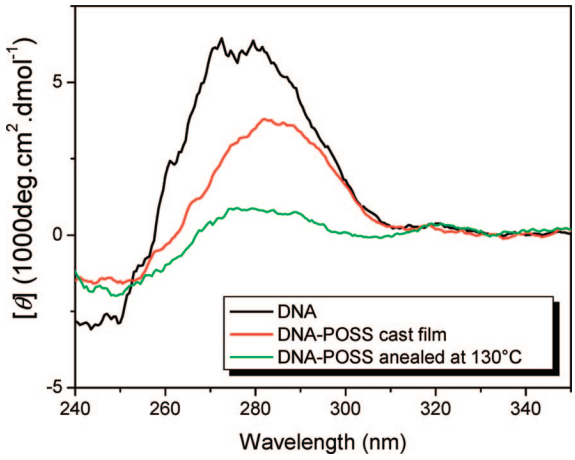


**Figure 8. Thin film circular dichroism spectra of DNA (black), DNA−POSS imidazolium salt complex cast from chloroform (red), and DNA−POSS annealed at 130 °C for 2 h (green). The film thicknesses were around 5 μm.**

uted to reflections from the residue shear-oriented hexagonal phase because of an incomplete transformation to the lamellar phase upon annealing at 130 °C.

Real-space observations of the inverted hexagonal and lamellar phases are shown in transmission electron microscopy (TEM) micrographs in Figure 7. Figure 7A shows the side-view of hexagonally packed DNA cylinders and the head-on view is shown in the inset. The samples were stained by uranyl acetate, which preferentially stained DNA moieties. In the head-on view, the dark DNA cross-section had a diameter of *ca.* 2−3 nm, consistent with the reported diameter of double-stranded DNA helices. Figure 7B shows the lamellar morphology of the DNA−POSS imidazolium salt complex slowly crystallized at 130 °C. Clearly, alternating dark DNA and bright POSS layers were seen. The bright POSS layers had an average thickness of 2.8 nm, which was nearly the same as the value calculated before.[26]

The conformation of DNA double-stranded helices was studied by circular dichroism (CD) spectroscopy, as shown in Figure 8. The Cotton effect in the pure DNA thin film had a positive peak around 278 nm, suggesting the B-form conformation.[21,29] For the DNA−POSS imidazolium salt complex cast from chloroform, an inverted hexagonal phase was obtained (see Figure 2A), and the Cotton effect weakened and slightly shifted to 282 nm, suggesting merely a slight distortion of the DNA helical conformation. For the DNA−POSS imidazolium salt complex annealed at 130 °C, most of the inverted hexagonal phase transformed into the lamellar phase. The Cotton effect was substantially suppressed, suggesting that the helical conformation in the double-stranded DNA was destroyed after the ionic complexation of POSS imidazolium salts at both sides of a DNA double helix. This is similar to the results reported before for DNA−triphenylene imidazolium salt complexes.[29]

In conclusion, we studied the self-assembled phase morphology and DNA conformation in a DNA complex with cationic POSS imidazolium salt. When POSS imidazolium salt complexed with double-stranded DNA, an inverted hexagonal phase resulted above the melting point of POSS crystals, owing to the negative spontaneous curvature of the POSS imidazolium cationic lipid. Competition between lamellar crystallization and negative spontaneous curvature of the POSS imidazolium lipid determined the self-assembled phase morphology in the sample. When the crystallization was relatively slow (*e.g.*, isothermal crystallization at 130 °C), crystallization of POSS molecules predominated the self-assembly process, and thus a lamellar phase was obtained. When the crystallization happened very fast (*e.g.*, quenched to 0 °C), lipid negative curvature predominated the self-assembly process, and the inverted hexagonal phase was retained with POSS lamellar crystals growing in the interstitials of DNA cylinders. Intriguingly, double-stranded DNA adopted the B-form helical conformation in the inverted hexagonal phase, whereas the helical conformation was largely de-

stroyed in the lamellar phase. We speculate that the ionic complexation of POSS crystals at both sides of the DNA double strand was the driving force to destroy the helical conformation of DNA.

## METHODS

DNA−POSS imidazolium salt complex was prepared in a similar way as other DNA−imidazolium salt complexes reported elsewhere.[17,29] Detailed synthesis and procedures for X-ray diffraction, TEM, and other characterizations are described in the Supporting Information.

*Acknowledgment.* This work was supported by NSF CAREER Award DMR-0348724, DuPont Young Professor Grant, 3M Nontenured Faculty Award, and Natural Science Foundation of China (20528405). We appreciate help from Mr. Michael R. Duff and Prof. Challa V. Kumar in the Chemistry Department at the University of Connecticut for CD measurements. The synchrotron X-ray experiments were carried out at the National Synchrotron Light Source, Brookhaven National Laboratory, supported by the U.S. Department of Energy. Help from Dr. Lixia Rong and Prof. Benjamin Hsiao at the State University of New York at Stonybrook for synchrotron X-ray experiments is highly acknowledged.

*Supporting Information Available:* Materials, characterization methods, composition determination for the DNA−POSS imidazolium salt complex, and supramolecular self-assembly of neat POSS imidazolium lipid. This information is available free of charge *via* the Internet at http://pubs.acs.org.

## REFERENCES AND NOTES

1. Vaillant, C.; Audit, B.; Thermes, C.; Arneodo, A. Influence of the Sequence on Elastic Properties of Long DNA Chains. *Phys. Rev. E* **2003**, *67*, 032901.
2. Elgin, S. C. R.; Workman, J. L. *Chromatin Structure and Gene Expression*. Oxford University Press: New York, 2000.
3. Tranchant, I.; Thompson, B.; Nicolazzi, C.; Mignet, N.; Scherman, D. Physicochemical Optimization of Plasmid Delivery by Cationic Lipids. *J. Gene Med.* **2004**, *6*, S24−S35.
4. Baysal, B. M.; Karasz, F. E. Coil-Globule Collapse in Flexible Macromolecules. *Macromol. Theory Simul.* **2003**, *12*, 627–646.
5. Kato, T.; Mizoshita, N.; Kishimoto, K. Functional Liquid-Crystalline Assemblies: Self-Organized Soft Materials. *Angew. Chem., Int. Ed.* **2006**, *45*, 38–68.
6. Ewert, K. K.; Evans, H. M.; Zidovska, A.; Bouxsein, N. F.; Ahmad, A.; Safinya, C. R. A Columnar Phase of Dendritic Lipid-Based Cationic Liposome-DNA Complexes for Gene Delivery: Hexagonally Ordered Cylindrical Micelles Embedded in a DNA Honeycomb Lattice. *J. Am. Chem. Soc.* **2006**, *128*, 3998–4006.
7. Rädler, J. O.; Koltover, I.; Salditt, T.; Safinya, C. R. Structure of DNA−Cationic Liposome Complexes: DNA Intercalation in Multilamellar Membranes in Distinct Interhelical Packing Regimes. *Science* **1997**, *275*, 810–814.
8. Artzner, F.; Zantl, R.; Rapp, G.; Radler, J. O. Observation of a Rectangular Columnar Phase in Condensed Lamellar Cationic Lipid-DNA Complexes. *Phys. Rev. Lett.* **1998**, *81*, 5015–5018.
9. Koynova, R.; MacDonald, R. C. Columnar DNA Superlattices in Lamellar o-Ethylphosphatidylcholine Lipoplexes: Mechanism of the Gel-Liquid Crystalline Lipid Phase Transition. *Nano Lett.* **2004**, *4*, 1475–1479.
10. Koltover, I.; Salditt, T.; Rädler, J. O.; Safinya, C. R. An Inverted Hexagonal Phase of Cationic Liposome-DNA Complexes Related to DNA Release and Delivery. *Science* **1998**, *281*, 78–81.
11. Zuhorn, I. S.; Hoekstra, D. On the Mechanism of Cationic Amphiphile-Mediated Transfection. To Fuse or not to Fuse: is that the Question. *J. Membr. Biol.* **2002**, *189*, 167–179.
12. Koiwai, K.; Tokuhisa, K.; Karinaga, R.; Kudo, Y.; Kusuki, S.; Takeda, Y.; Sakurai, K. Transition from a Normal to Inverted Cylinder for an Amidine-Bearing Lipid/pDNA Complex and its Excellent Transfection. *Bioconjug. Chem.* **2005**, *16*, 1349–1351.
13. Krishnaswamy, R.; Pabst, G.; Rappolt, M.; Raghunathan, V. A.; Sood, A. K. Structure of DNA−CTAB−Hexanol Complexes. *Phys. Rev. E.* **2006**, *73*, 031904.
14. Krishnaswamy, R.; Raghunathan, V. A.; Sood, A. K. Reentrant Phase Transitions of DNA−Surfactant Complexes. *Phys. Rev. E.* **2004**, *69*, 031905.
15. Leal, C.; Bilalov, A.; Lindman, B. Phase Behavior of a DNA-Based Surfactant Mixed with Water and *n*-Alcohols. *J. Phys. Chem. B* **2006**, *110*, 17221–17229.
16. Smisterova, J.; Wagenaar, A.; Stuart, M. C.; Polushkin, E.; ten Brinke, G.; Hulst, R.; Engberts, J. B.; Hoekstra, D. Molecular Shape of the Cationic Lipid Controls the Structure of Cationic Lipid/Dioleylphosphatidylethanolamine-DNA Complexes and the Efficiency of Gene Delivery. *J. Biol. Chem.* **2001**, *276*, 47615–47622.
17. Cui, L.; Zhu, L. Lamellar to Inverted Hexagonal Mesophase Transition in DNA Complexes with Calamitic, Discotic, and Cubic Shaped Cationic Lipids. *Langmuir* **2006**, *22*, 5982–5985.
18. Mel'nikova, Y. S.; Lindman, B. pH-Controlled DNA Condensation in the Presence of Dodecyldimethylamine Oxide. *Langmuir* **2000**, *16*, 5871–5878.
19. Hsu, W. L.; Chen, H. L.; Liou, W.; Lin, H. K.; Liu, W. L. Mesomorphic Complexes of DNA with the Mixtures of a Cationic Surfactant and a Neutral Lipid. *Langmuir* **2005**, *21*, 9426–9431.
20. Hsu, W. L.; Li, Y. C.; Chen, H. L.; Liou, W.; Jeng, U. S.; Lin, H. K.; Liu, W. L.; Hsu, C. S. Thermally-Induced Order−Order Transition of DNA−Cationic Surfactant Complexes. *Langmuir* **2006**, *22*, 7521–7527.
21. Tanaka, K.; Okahata, Y. A DNA−Lipid Complex in Organic Media and Formation of an Aligned Cast Film. *J. Am. Chem. Soc.* **1996**, *118*, 10679–10683.
22. Zhou, S.; Liang, D.; Burger, C.; Yeh, F.; Chu, B. Nanostructures of Complexes Formed by Calf Thymus DNA Interacting with Cationic Surfactants. *Biomacromolecules* **2004**, *5*, 1256–1261.
23. Caracciolo, G.; Pozzi, D.; Amenitsch, H.; Caminiti, R. Multicomponent Cationic Lipid−DNA Complex Formation: Role of Lipid Mixing. *Langmuir* **2005**, *21*, 11582–11587.
24. Francescangeli, O.; Pisani, M.; Stanic, V.; Bruni, P.; Weiss, T. M. Evidence of an Inverted Hexagonal Phase in Self-Assembled Phospholipid−DNA−Metal Complexes. *Europhys. Lett.* **2004**, *67*, 669–675.
25. Liang, H. J.; Harries, D.; Wong, G. C. L. Polymorphism of DNA−Anionic Liposome Complexes Reveals Hierarchy of Ion-Mediated Interactions. *Proc. Natl. Acad. Sci. U.S.A.* **2005**, *102*, 11173–11178.
26. Miao, J.; Cui, L.; Lau, H. P.; Mather, P. T.; Zhu, L. Self-Assembly and Chain-Folding in Hybrid Coil-Coil-Cube Triblock Oligomers of Polyethylene-*b*-Poly(ethylene oxide)-*b*-Polyhedral Oligomeric Silsesquioxane. *Macromolecules* **2007**, *40*, 5460–5470.
27. Cui, L.; Collet, J. P.; Xu, G. Q.; Zhu, L. Supramolecular Self-Assembly in a Disk-Cube Dyad Molecule based on Triphenylene and Polyhedral Oligomeric Silsesquioxane (POSS). *Chem. Mater.* **2006**, *18*, 3503–3512.
28. Zhu, L.; Calhoun, B. H.; Ge, Q.; Quirk, R. P.; Cheng, S. Z. D.; Thomas, E. L.; Hsiao, B. S.; Yeh, F.; Liu, L. Z.; Lotz, B. Initial-Stage Growth Controlled Crystal Orientations in Nanoconfined Lamellae of a Self-Assembled Crystalline-Amorphous Diblock Copolymer. *Macromolecules* **2001**, *34*, 1244–1251.
29. Cui, L.; Miao, J. J.; Zhu, L. Spacer Length Controlled Oblique-Columnar to Lamello-Columnar Mesophase Transition in Liquid Crystalline DNA−Discotic Cationic Lipid Complexes. *Macromolecules* **2006**, *39*, 2536–2545.